Chapter 5

Carbonylative Cycloaddition of Allyl Halides and Acetylenes Promoted by $Ni(CO)_4$. A Study on the Reaction Mechanism

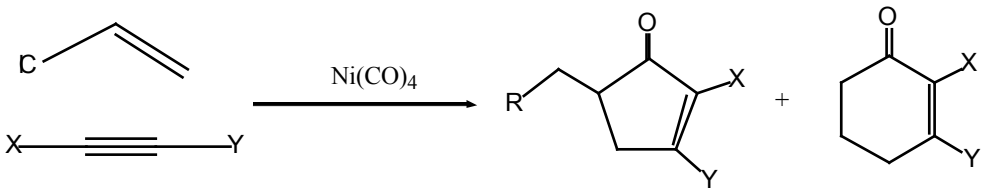

The [2+2+1] carbonylative cycloaddition of allyl halides and acetylenes promoted by $Ni(CO)_4$ is an elegant route to synthesize cyclopentenones and other cycled and linear products. This chapter presents the results of a DFT study on a proposed reaction mechanism, the energy profile for which was established by determining the structures and relative energies of the putative intermediates involved. The energy barriers for the most important steps were also determined. The allyl and the alkyne moieties can be coupled by π- or σ-allyl complexes, although the π-allyl reaction pathway is found to be less energetically demanding. The energy barrier for cyclopentenone formation is lower than for cyclohexenone, in agreement with the experimental findings. Acetylene substituents have a noteworthy effect on the process regioselectivity and this is manifested as a kinetic effect in the computed energy barriers. The yield in five- or six-member rings has a thermodynamic origin but also depends on the energy barrier when substituted allyls are used.

5.1 INTRODUCTION

The metal promoted carbonylative cycloaddition reaction involving one alkene, one alkyne and carbon monoxide is one of the most convergent means for synthesizing cyclopentenone skeletons.[1] The cyclopentenone formation reaction can be regarded as a formal [2+2+1] cycloaddition in which the alkyne and the alkene moieties serve as two-carbon components, and the carbonyl functionality is supplied from one of the carbonyl ligands of the metal unit. Since the discovery of the carbonylative cycloaddition of allyl halides and alkynes with $Ni(CO)_4$ by Chiusoli[2] and the Pauson-Khand reaction[3] ($M_n(CO)_n$=$Co_2(CO)_6$) in the early 1970s, it has been found that many other transition metal complexes can undergo cyclocondensations: Ti,[4] Zr,[5] Mo,[6] W,[7] Fe,[8] Ru,[9] Ni,[10] and very recently Rh[11]. Among these methods, the Pauson-Khand reaction stands out because of its experimental simplicity, functional group compatibility and predictable regio- and stereochemical outcome and it is still a very active research field.[9b,11,12]

The Chiusoli reaction has been widely studied by Moretó et al.[10a,13a-d] and others.[13e] The reaction can afford higher degrees of regio- and stereoselectivity than the Pauson-Khand reaction, but it is not very popular among chemists, probably because it uses the hazardous $Ni(CO)_4$. The factors, which affect the yield of different products, have also been systematically studied. The solvent was found to have considerable influence on the yield, and alcohols or water must be present in all cases. Alkyne substituents had a dramatic influence on product distribution: monosubstituted acetylenes gave predominantly linear products whereas disubstituted acetylenes produced cyclopentenones. In the latter case, the regioselectivity depends on the alkyne triple bond polarization if steric effects are not very demanding. A mechanism which involves π-allyl nickel complexes has been proposed to explain the products obtained.[13b,c] Very recently, it has been reported that cyclopentenones can be efficiently and selectively obtained in a single operative protocol which does not handle nickel tetracarbonyl but uses $Ni(COD)_2$ instead to prepare the required π-allyl nickel complex directly.[14]

Density Functional Theory (DFT) based methods have emerged as a practical tool in studies of organometallic energetics and kinetics[15] as can be seen by the number of papers appeared which have been published in recent years on organometallic reactivity and catalysis.[16] However, to the best of our knowledge, this kind of organometallic reaction has not been studied yet by computational methods.

The main goal of this work is to use DFT methods to propose a mechanism for the Chiusoli reaction compatible with the products obtained. To achieve this objective, acetylene and allyl chloride were considered as models of alkynes and allyl halides and the reaction intermediates and main transition states were determined. On the basis of the results obtained for this simple system, acetylene and allyl substituents effects were analyzed.

5.2 COMPUTATIONAL DETAILS AND TEST CALCULATIONS

All calculations based on DFT methodology were performed with DGauss[17a] and Gaussian94[17b] codes. The basis sets used were the DZVP sets taken from the DGauss library,[18] and were all electron Gaussian type basis sets of split valence plus polarization quality. The size of the basis set was (5s) for H, (9s,5p,1d) for C and O, and (12s,8p,1d) for Cl, contracted into [2], [3,2,1] and [4,3,1], respectively. The basis set for Ni was a (15s,9p,5d) set contracted into [5,3,2]. DFT calculations were done in a self consistent manner by using the form given by Vosko, Wilk and Nusair[19] for the local part of the exchange-correlation potential and the gradient corrected exchange term proposed by Becke[20] and the gradient corrected correlation term proposed by Lee, Yang and Parr[21] (BLYP functional). Geometry optimizations were carried out without any symmetry restrictions. Some intermediates and transition state structures were characterized by means of normal modes analysis. In these cases, the zero point energy (ZPE) was evaluated at the BLYP level. All BLYP calculations were carried out with DGauss. It has been recently demonstrated[22] that the use of hybrid functionals, i.e., functionals that include some portion of Hartree-Fock exchange, improve the metal-ligand bond dissociation energies, especially if the metal atom state changes during the dissociation. Among the several hybrid functionals that has been developed, the B3LYP[23] is nowadays the most widely used. In order to check the reliably of the BLYP energies, B3LYP single point calculations on the BLYP optimized geometries (B3LYP//BLYP) were performed with Gaussian94 on the most important structures using the same DZVP basis sets. The topological properties of the electronic charge density[24] were investigated using Xaim[25] and a version of the AIMPAC package.[26] Atomic charges for uncoordinated substituted alkynes were determined by means of two methods: NPA (Natural Population Analysis)[27] and Mulliken[28] using the Gaussian94 code[17b] with the DZVP basis sets and the BLYP functional.

Although it is well known that current DFT methods are quite accurate in determining geometries and reaction energies, test calculations were carried out on

$Ni(CO)_4$ and $Ni(allyl)_2$ in order to assess the quality of the methods used. These simple systems were chosen because accurate experimental data are available and because they cover the two principal metal oxidation states in the reaction being studied, namely Ni(0) and Ni(II).

For $Ni(CO)_4$, both solid-state[29a] and gas-phase[29b] tetrahedral geometries were determined. The gas phase Ni–C and C–O distances (which are directly comparable with our calculations) are 1.838 and 1.141 Å, respectively. We determined the Ni–C bond length to be 1.848 Å, 0.01 Å longer than the experimental value, whereas for the C–O bond our computed value is 1.164 Å (0.023 Å longer). These small discrepancies are similar to the values previously computed by Ziegler[30] using the same methodology. We computed the first CO dissociation energy to be 24.8 $kcal.mol^{-1}$ at the BLYP level and 23.5 $kcal.mol^{-1}$ at the B3LYP//BLYP. In this case, both values are in excellent agreement with the experimental measure reported by Stevens et al.[31] (25 ± 2 $kcal.mol^{-1}$) and also with a value previously computed by Ziegler et al.[30] Goddard[32] determined a very low temperature neutron diffraction structure for $Ni(allyl)_2$, being the three Ni–C bond distances 2.026, 1.979 and 2.030 Å and the two C–C bond distances 1.416 and 1.413 Å. Our computed values are 2.055, 2.001 and 2.055 Å for the Ni–C bonds and 1.428 Å for the two C–C bonds. The reader can observe how all distances are slightly longer but the trend showed by the Ni–C bonds is very well reproduced. The results for these two test systems give us confidence in the method used.

5.3 THE REACTION MECHANISM

Moretó et al.[13] proposed a mechanism to explain the products obtained and concluded that a π-allyl nickel complex is formed at an early stage of the reaction. This mechanism consists of the following steps: formation of a (π-allyl)nickel species, coordination of the acetylene moiety, creation of the new C_{allyl}-$C_{acetylene}$ bond, carbonyl insertion, and ring closing to form either five- or six-member rings, mainly cyclopentenones and cyclohexenones. In this study, we have explored the different steps that presumably constitute the overall mechanism, but also the possibility that σ-allyl species might be involved in some of them.

5.3.1 Formation of the Active Ni(II) Complex

When the reaction starts from allyl chloride and $Ni(CO)_4$, an oxidative addition is expected to occur. This step would produce a (π-allyl)Ni^{II} complex which can undergo the subsequent reactions and which must be able to coordinate

acetylene. We postulate that this complex might plausibly be Ni(π-allyl)(CO)Cl, (**1**), which is the product of the reaction:

$$Ni(CO)_4 + CH_2{=}CH\text{-}CH_2Cl \rightarrow Ni(\eta^3\text{-}CH_2CHCH_2)COCl\ (\mathbf{1}) + 3CO \qquad (\mathbf{5.1})$$

The formation of complex **1** is not obvious, is coupled to some carbonyl dissociation and takes place in three steps. We explored in detail some intermediates and found that the least energetic pathway could involve the product of the coordination of allyl chloride to $Ni(CO)_4$ by dissociating a carbonyl ligand. In the first step, allyl chloride can coordinate to $Ni(CO)_3$ giving a tetrahedral $Ni(\eta^2\text{-}CH_2{=}CH\text{-}CH_2Cl)(CO)_3$ complex. The energetic cost to reach this complex plus a free carbonyl molecule amounts 18.3 kcal.mol^{-1} at the BLYP level (15.8 kcal.mol^{-1} at the B3LYP//BLYP level). The optimized structure of $Ni(\eta^2\text{-}CH_2{=}CH\text{-}CH_2Cl)(CO)_3$ complex is tetrahedral being the Ni-C_{alkene} distances 2.292 and 2.245 Å and the C=C bond length 1.382 Å. The three Ni-carbonyl bond lengths are 1.823, 1.825 and 1.848 Å. The longest Ni-carbonyl bond found corresponds to the carbonyl, which is closest to the chloride atom. Note that this carbonyl is the ligand that is going to dissociate when the oxidative addition takes place. Therefore, it seems plausible that the second step is the oxidative addition, which occurs in a concerted manner with the loss of one carbonyl ligand and produces the $Ni(\pi\text{-allyl})(CO)_2Cl$ complex, **2**. This step is also endothermic (21.8 kcal.mol^{-1} BLYP; 18.5 kcal.mol^{-1} B3LYP//BLYP). Finally, the third step is the loss of another carbonyl from the saturated complex **2** to form the unsaturated complex **1**. To dissociate the third carbonyl a small amount of energy (7.2 kcal.mol^{-1} BLYP; 3.8 kcal.mol^{-1} B3LYP//BLYP) is still required.

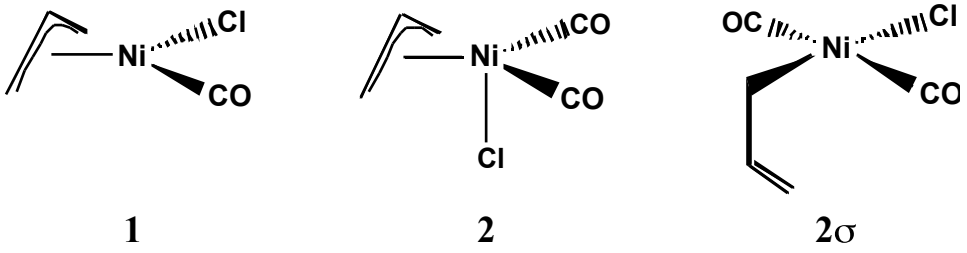

1 **2** **2σ**

Scheme 5.1

Complex **1** was spectroscopically detected by other authors in related reactions.[33] Similar complexes, in which the carbonyl ligand is replaced by phosphines, are known and their structures have been determined by X-ray diffraction. Brandes et al.[34] and Carmona et al.[35] have shown that these complexes

have a slightly distorted square-planar geometry, in which the allyl ligand coordinates in a π manner and occupies two coordination sites. We postulate that **1** and **2** might be the π-allyl complexes formed at an early stage of the reaction. The energy required to obtain these complexes is not low, but as we will describe later, the overall reaction is highly exothermic and the reaction path based on these π-allyl complexes satisfactory justify the products obtained and also their distribution. On the other hand, the experimental conditions required to carry out the oxidative addition are consistent with our findings. The reaction must be performed with coordinative solvents (methanol or acetone) to help CO dissociation and at 40°C if $Ni(CO)_4$ is used.[13b] If $Ni(COD)_2$ is used instead of $Ni(CO)_4$, neither heating nor induction time are required, since the COD ligand is more labile than carbonyl and the oxidative addition takes places immediately.[14]

We also explored a dissociative path, involving successive carbonyl dissociations to $Ni(CO)_2$, which could undergo the oxidative addition, but this path is found to be more energetically demanding that the concerted path.

The computed geometries for **1** and **2** (Scheme 5.1) are shown in Figure 5.1. A square-planar structure for **1** and square-based pyramid for **2** are easily recognized. To compare the geometries obtained for these intermediates with those obtained experimentally, the Cambridge Structural Database System (CSD)[36] was searched for related systems. The search produced five hits for Ni-π-allyl X-ray structures that have Ni-C_{allyl} bond distances between 1.939Å and 2.089Å. In comparison with **1** and **2**, these values indicate that the computed values are slightly larger than the greatest value reported. Known allyl C-C bond lengths range from 1.309 to 1.421 Å, whereas the values found for **1** and **2** are located in the upper zone of this range. Nickel carbonyl bond distances fall into the range of 85 known structures in the CSD that have values from 1.676Å to 1.866Å. Nickel-chloride bond lengths range from 2.121 to 2.701Å in 295 structures found in CSD. The computed values of the Ni-Cl distance in **1**(2.217 Å) and **2** (2.408 Å) are within this range.

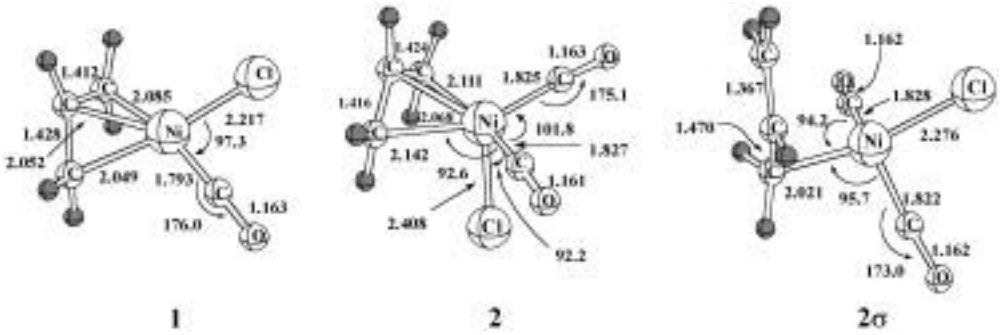

Figure 5.1. Selected geometric parameters for **1**, **2** and **2**σ.

Complex **2** may be in equilibrium with a σ-allyl complex **2**σ, i.e., a formal 16-electron species. The structure and main geometric parameters obtained for **2**σ are shown in Figure 5.1. This tetracoordinated complex has a distorted structure that is more similar to a tetrahedron than to a square planar coordination. The carbonyl-nickel-carbonyl angle is 138.4°, a long way from the linear value, whereas the σ-carbon-nickel-chloride is 162.6°. This distorted structure was obtained from a square planar starting point in the geometry optimization process. The spatial orientation of allyl and its C-C bond lengths clearly indicate that it is coordinated as in the σ mode. Note that whereas the nickel carbonyl bond lengths are only slightly different from their values in **2**, the Ni-Cl bond in **2**σ is shorter. The computed energy difference between **2** and **2**σ is found to be only 0.75 kcal.mol^{-1} (at the BLYP level), which means that σ-allyl species may be involved in the reaction mechanism.

5.3.2 $C_{acetylene}$–C_{allyl} Bond Making

In this step the first new carbon-carbon bond is formed between acetylene and the coordinated allyl. This a crucial step in determining the regioselectivity of the final product if asymmetrically disubstituted acetylenes are used, because the products obtained will depend on which acetylenic carbon the allyl will attack. The results presented in the section above show that this step can follow two different reaction pathways: from complex **1** with π-allyl species or from complex **2**σ with σ-allyl intermediates.

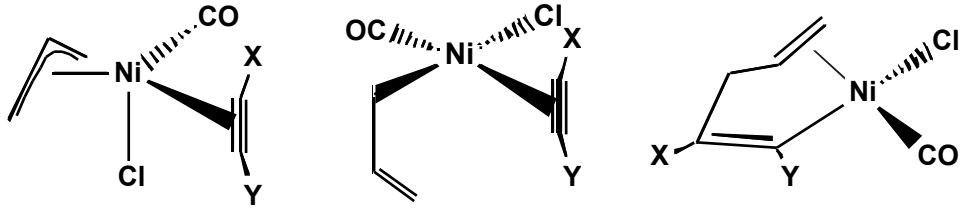

3 **3**σ **4**

Scheme 5.2

In the π-allyl species, an intermediate may be formed between **1** and acetylene. This intermediate is the 18-electron Ni(II) pentacoordinated complex **3** (Scheme 5.2). Alternatively, a concerted process could also be possible from **2** consisting in CO dissociation and acetylene coordination. The geometry for this complex (see Figure 5.2) is equivalent to a square-based pyramid, in which the chloride ligand occupies the apical position. This type of structure is not unknown in Ni(II)

chemistry and can be found, for example, in the Ni(μ^3-2-methylallyl)($Ph_2PCH_2CH_2PPh_2$)Br complex.[37] The geometric parameters found for the nickel-acetylene framework agree well with the ones reported. The Ni-$C_{acetylene}$ bonds of the 14 structures in the CSD system range from 1.862 to 2.063Å, but our computed values are slightly longer. The values that have been reported for the C-C bond are between 1.233 and 1.276 Å, and our value is in this range. We compute that the acetylene coordination process is somewhat endothermic. The energy required to form complex **3** from **1** amounts to 5.4 kcal.mol^{-1} at the BLYP level (7.8 kcal.mol^{-1} at the B3LYP//BLYP level). Other isomers for complex **3** were also considered, but all of them appeared unstable and led to dissociative products. Complex **3** can easily afford the transition state **TS1** shown in Figure 5.2. Normal modes analysis unambiguously assigns this structure as a transition state, with only one imaginary frequency (–323 cm^{-1}) corresponding to the reaction coordinate, i.e., the stretching of the new carbon-carbon bond. The geometry of the transition state shows that the allyl ligand is slightly modified and that the new C-C bond is still long. The energy required to reach this transition state from **3** is 13.0 kcal.mol^{-1} at the BLYP level (14.3 kcal.mol^{-1} at the B3LYP//BLYP level).

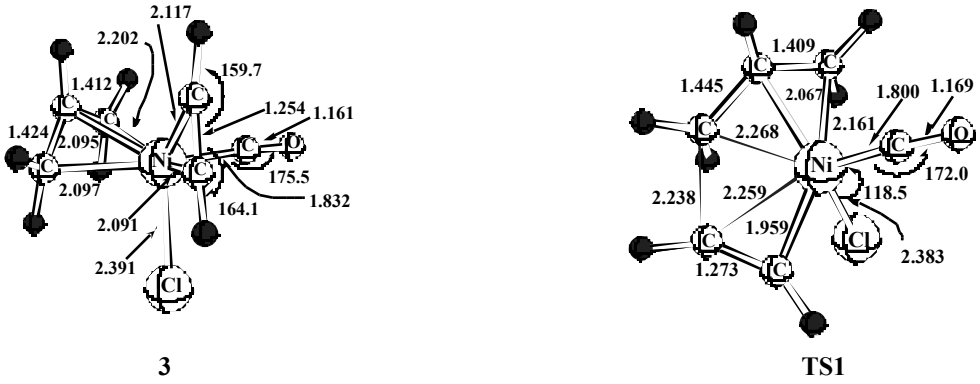

Figure 5.2. Selected geometric parameters for **3** and **TS1**.

It is easy to imagine that **3** transforms into **TS1** when acetylene rotates around the axis that passes through the C-C midpoint and the Ni atom. In fact, we have computed an approximation to the acetylene rotation barrier (see Figure 5.3). The curve is an approximation because the geometry was kept fixed at each point, and thus, it is an overestimation of the true curve. The maximum energy point in the reaction coordinate is at 90°, approximately, and is 14 kcal.mol^{-1} higher than **3** (at the BLYP level). If we compare this value with the energy difference between **3**

and the transition state, **TS1**, we believe that is reasonable to assume that the transition state is reached by an acetylene rotation.

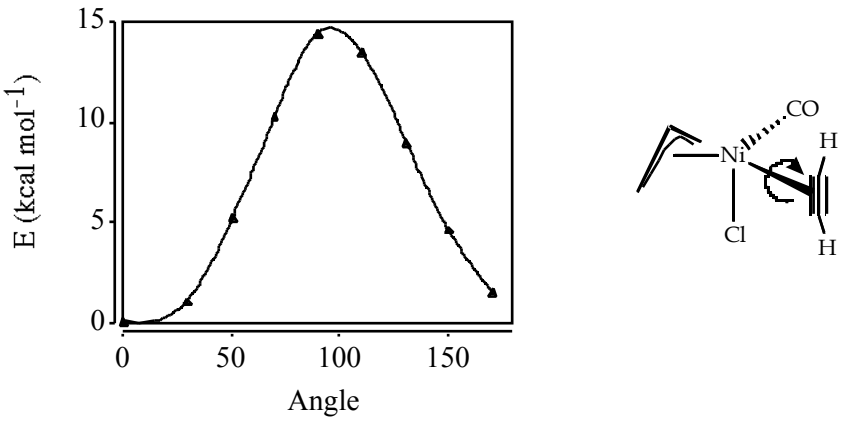

Figure 5.3. Energy profile for the acetylene rotation in **3**.

As we have suggested above, there may be another way of making the $C_{acetylene}$-C_{allyl} bond using σ-allyl species. If this is so, we would have to find an alternative to the **2** →**1** →**3** →**TS1** route starting from complex **2**σ. Of course **2** is coordinatively saturated whereas complex **2**σ is not; thus, acetylene could directly coordinate to **2**σ to form a pentacoordinated 18e complex. Despite our work to determine an optimized geometry for Ni(σ-allyl)$(CO)_2$(acetylene)Cl structures, we found no evidence of pentacoordinated σ-allyl complexes. Therefore, we concluded that there is enough space for acetylene to coordinate in the σ-allyl complex **2**σ but that it does not proceed. If it is to do so, a carbonyl must be replaced by the incoming ligand.

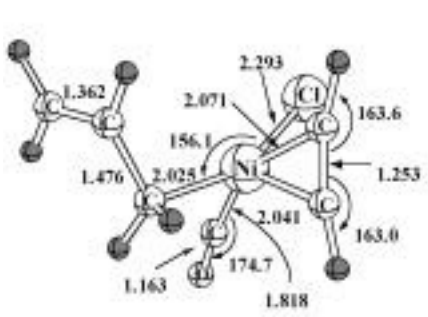

3σ

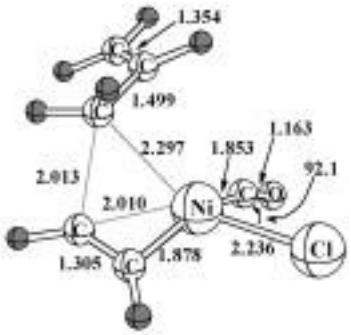

TS1σ

Figure 5.4. Selected geometric parameters for **3**σ and **TS1**σ.

Assuming this hypothesis, a Ni(σ-allyl)(CO)(acetylene)Cl structure, **3**σ, was characterized (see Figure 5.4) by dissociating one carbonyl from complex **2**σ and subsequently coordinating acetylene. This process is evaluated to be also endothermic by 14.1 kcal.mol^{-1}(BLYP level). This value corresponds to the formation of one of three possible isomers. Another isomer (acetylene trans to chloride) was found to be 4.2 kcal.mol^{-1} less stable than **3**σ (BLYP level). The third possible isomer would have σ-allyl and acetylene in trans, and so they would not be able to couple. These structures are equivalent to **2**σ in the sense that they are all distorted tetracoordinated geometries. This step means that the product of CO dissociation from **2**σ should be considered formally as a 14e complex. Although it has not been studied in detail, it should be very unstable and would probably easily transform to the 16e π-allyl complex **1**. This reasoning means that the energetic cost of reaching **3**σ from **2**σ would be considerable and that the σ-allyl route would be inaccessible. However, just as **2** and **2**σ are in π-allyl/σ-allyl equilibrium, complex **3**σ can also be reached from **3** since complex **3**σ is only 3.3 kcal.mol^{-1} (6.5 kcal.mol^{-1} at the B3LYP//BLYP level) less stable than **3** . Following a σ-allyl route, the transition state for the $C_{acetylene}$-C_{allyl} bond making, **TS1**σ, is 17.3 kcal.mol^{-1}(16.9 kcal.mol^{-1} at B3LYP//BLYP) above **3**σ. These results show that the σ-allyl pathway is always more energetically demanding than the π-allyl one, but the energy difference between both reaction paths is not too great (7.5 kcal.mol^{-1} at the BLYP level and 9.1 kcal.mol^{-1} at the B3LYP//BLYP level).

The geometry of the transition state structure **TS1**σ is shown in Figure 5.4. The coordinated allyl and acetylene have not changed their internal parameters appreciably and still retain their own bonding pattern. The disymmetric coordination of acetylene and the elongation of the C_{allyl}-nickel bond length are the most noteworthy changes undergone by **3**σ. Note that the length of the C_{ac}-C_{ac} bond is midway between the values for the reactant, **3**σ, and the product, **4**. All the other parameters have slightly changed towards the value that they will have in the product. The structures of the two equivalent transition states, **TS1** and **TS1**σ (Figure 5.2 and 5.4, respectively) differ in several parameters: the C-C forming bond as well as the two Ni-acetylene bonds are longer in **TS1**, and consequently the acetylene C-C bond is shorter. It is worth noting that the topology of the charge density distribution, ρ(r), computed for the TS structures **TS1** and **TS1**σ, suggests that all newly forming bonds are already formed. In fact, bond critical points in ρ(r) have been characterized in the TS structures for all making and breaking bonds.

Once the transition states **TS1** or **TS1σ** are reached, the system proceeds towards the same metallacycle intermediate, **4**. The structure of complex **4**, (Figure 5.5), is an almost perfect square-planar geometry and the bonding pattern that emerges from it clearly indicates that the acetylene triple bond has become double, whereas the other double bond corresponding to the allyl is coordinated to the metal in a π manner. Complex **4** is 4.0 kcal.mol^{-1} (at the BLYP level) more stable than the other possible isomer. The CSD system[36] shows 35 hits for structures containing Ni-η^2-alkene, which range from 1.954 to 2.080 Å. The corresponding values reported for **4** are slightly longer than those measured experimentally.

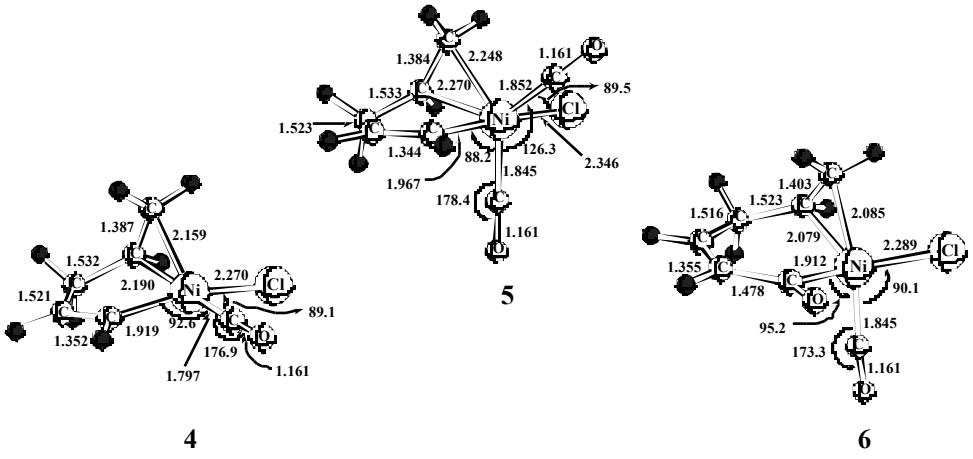

Figure 5.5. Selected geometrical parameters for **4**-**6**.

It should be pointed out that the exothermicity of this step is considerable, for both the π-allyl and for the σ-allyl pathways. In fact, product **4** is more stable than reactant **3** by 34.4 kcal.mol^{-1} (35.6 kcal.mol^{-1} at the B3LYP//BLYP level) and more stable than reactant **3σ** by 37.7 kcal.mol^{-1} (42.1 kcal.mol^{-1} at the B3LYP//BLYP level).

5.3.3 Carbonyl Insertion

Once allyl and acetylene have been coupled onto the metal coordination sphere a carbonyl still needs to be inserted into the metal-carbon bond before the cycle can be closed and a cyclopentenone or cyclohexenone formed. Our hypothesis is that carbonyl inserts into the metal-vinyl bond.

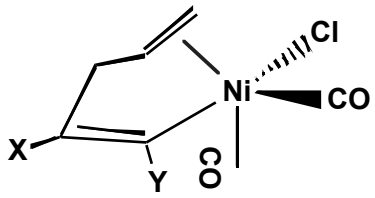

5

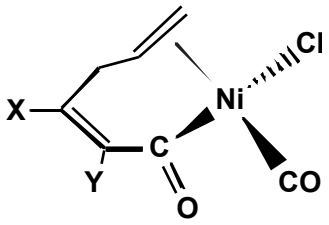

6

Scheme 5.3

The carbonyl could be inserted into the vinyl-Ni bond from complex **4**, in which one carbonyl ligand is cis-coordinated to the metal, but the resulting intermediate would be coordinatively unsaturated, and this involves considerable destabilization. Therefore, we propose an associative reaction path in which a new carbonyl ligand coordinates to the metal to form a pentacoordinated 18-electron Ni(II) species that evolves to a square planar 16-electron insertion product. In fact, we have been able to characterize complex **5** (Scheme 5.3) as the product of a carbonyl ligand coordinating to complex **4**.

Figure 5.5 shows that this intermediate has a square based pyramid structure, in which the new carbonyl occupies the apical position, and the former carbonyl and the chlorine have slightly bent away from the apex. This process is computed to be highly exothermic by 13.3 $kcal.mol^{-1}$ at BLYP level (10.1 $kcal.mol^{-1}$ at the B3LYP//BLYP). Figure 5.5 also shows that all the metal-ligand bond distances in **5** have increased from the values they had in **4**.

Insertion of a carbonyl into the metal-carbon bond leads to complex **6**, which is more stable than the reactant **5** by 12.1 $kcal.mol^{-1}$ at BLYP level (10.9 $kcal.mol^{-1}$ at the B3LYP//BLYP level), and which has a distorted square-planar structure shown in Figure 5.5. From this intermediate, the system is ready to proceed to ring closing by coupling the carbon carbonyl atom to one of the two ethylenic carbon atoms and form either cyclopentenone or cyclohexenone.

5.3.4 Closing the Ring

The metallacycle complex **6** is thus the common starting point which can lead to five- and six-membered rings. Before presenting the results, let us remark that complex **6** is formally a 16e system and that the product of the ring closure process is a three coordinated Ni(alkyl)(CO)Cl 14e species, which is coordinatively unsaturated and which would easily progress to a more stable 16e complex,

probably coordinating a CO molecule. We will refer to this path as *direct*. Alternatively, we could imagine a concerted ring closing-carbonyl coordination process, in which carbonyl coordination occurs while the ring closes and that this would produce the 16e Ni(alkyl)$(CO)_2$Cl cycled product. We will refer to this path as *concerted*. A third possibility involves an 18e species if the CO molecule coordinates to **6** before the ring closes, but in spite of our efforts, we have not been able to characterize such a structure.

5.3.4.1 Cyclopentenone Formation

Cyclopentenones form from complex **6** through the attack of the acyl carbon atom on the internal olefin carbon atom. Meanwhile, the Ni-acyl bond breaks and the Ni-terminal olefin carbon bond forms. We investigated the direct and concerted paths in Scheme 5.4, and located and characterized the transition state structures for each of the paths. The geometries of the intermediates **7** and **7a** and of the transition states **TS2** and **TS2a** are shown in Figure 5.6 and 5.7.

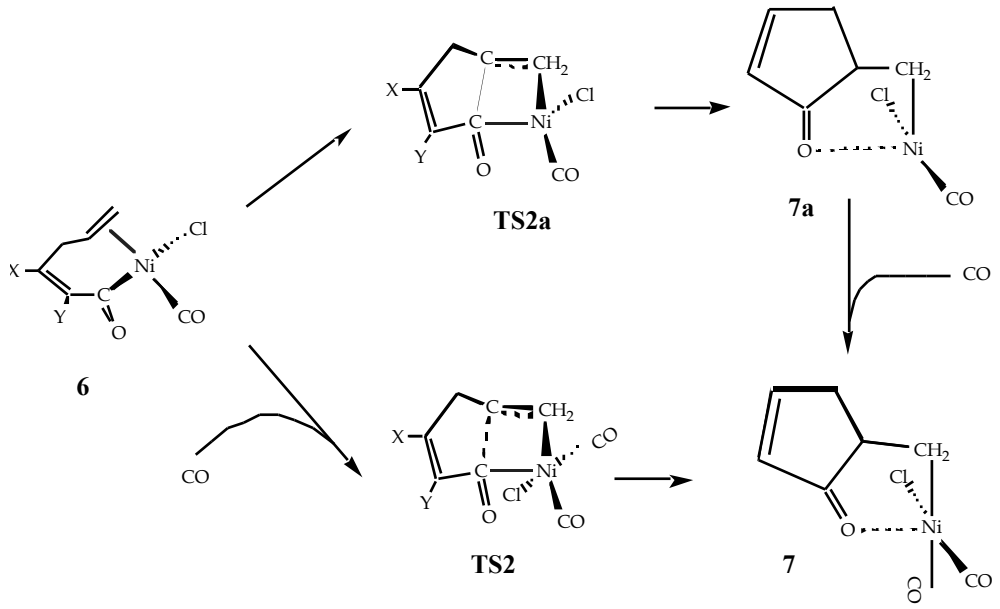

Scheme 5.4

The concerted path was found to have a lower energetic cost than the direct: the transition state structure **TS2** is only 6.1 kcal.mol^{-1} (8.0 kcal.mol^{-1} at the B3LYP//BLYP level) above complex **6** plus CO, whereas the energy necessary to

reach the transition state **TS2a** from complex **6** is 17.2 kcal.mol^{-1} (15.3 kcal.mol^{-1} at the B3LYP//BLYP level). Thus, the concerted path is favored in 11.1 kcal.mol^{-1} (7.3 kcal.mol^{-1} at the B3LYP//BLYP level) respect to the direct one. The overall process (carbonyl coordination and cyclopentenone formation) was exothermic by 16.8 kcal.mol^{-1} at the BLYP level and by 21.5 kcal.mol^{-1} at the B3LYP//BLYP level. In contrast, the product of the direct path, **7a**, was only 1.3 kcal.mol^{-1} less stable than the reactants at the BLYP level and 3.6 kcal.mol^{-1} more stable than the reactants at the B3LYP//BLYP level. It should be pointed out that the structures of products **7** and **7a** (Figure 5.6 and 5.7, respectively) both have an interesting feature: in the cyclopentenone ring, the carbonylic oxygen lone pair is located just over the nickel atom and may interact with it. This can be seen quite clearly if complex **7** is considered to have a square planar structure (formed by two carbonyls, the chloride atom and the alkylcyclopentenone ligand) in which the carbonylic oxygen occupies the apex of a square-based pyramid. It may be thought at first that the interaction with the nickel atom in complex **7a**, formally a 14e T-shaped structure, is necessary to stabilize the electronically unsaturated Ni(II) atom. However, the Ni-O distance in **7** (2.648 Å) is noticeably shorter than in **7a** (2.842 Å) and this indicates a stronger interaction. In **7a** this interaction is estimated[38] to be 4.5 kcal.mol^{-1} (at the BLYP level) and characterized by a bond critical point (bcp) in the electronic charge density. In complex **7** this interaction is even stronger and also manifested as a bcp in $\rho(r)$. The value of $\rho(r)$ at the bcp (0.014 au) is very low and indicates little interaction Ni-O. The value of the Laplacian of the charge density at the bcp (0.093 au) is also low and positive. Thus, according to the Theory of Atoms in Molecules,[24] the positive value of the Laplacian at the bcp indicates a closed shell interaction of electrostatic nature. The shorter Ni-O distance in **7** can be explained in this way, since the formal 16e Ni(II) in **7** is more positively charged than the 14e Ni(II) in **7a** and this is probably due to the π-back-donation to the additional carbonyl ligand in **7**. This kind of interaction is not experimentally unknown. In fact, the complex that best compares with **7** is the (Ni(di-methylphosphine)(alkyl)(Cl) characterized by Carmona et al.[39] in a X-ray study, which has a Ni-O distance of 2.535 Å. Other authors have also reported X-ray structures with shorter Ni-O distances, either intermolecular as for Carmona[40a] or with solvent molecules.[40b] The two transition states **TS2** and **TS2a** have similar structures for the reacting framework, and the forming C-C bond is longer in **TS2** than in **TS2a**. The same feature was found for the transition states **TS1** and **TS1**σ of the $C_{acetylene}$-C_{allyl} bond making process.

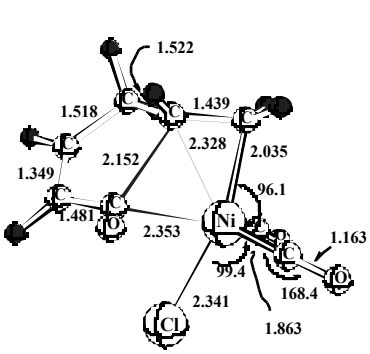

TS2

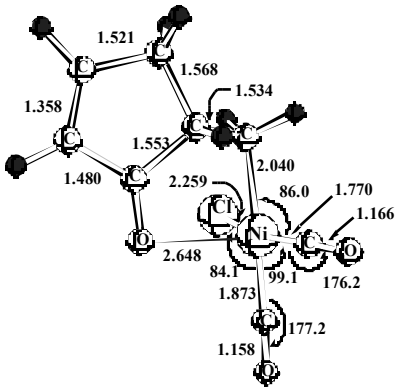

7

Figure 5.6. Selected geometric parameters for **TS2** and **7**.

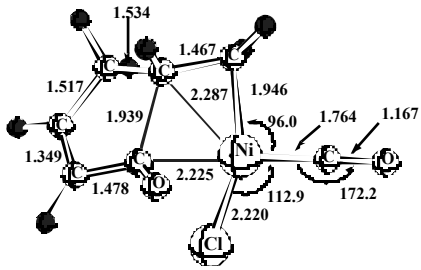

TS2a

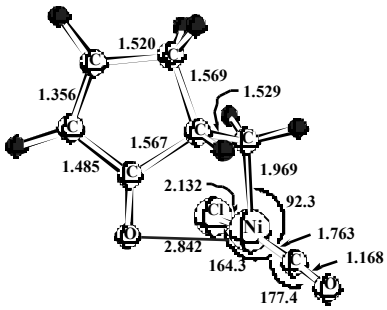

7a

Figure 5.7. Selected geometric parameters for **TS2a** and **7a**.

5.3.4.2 Cyclohexenone Formation

The process of forming of cyclohexenones from complex **6** (Scheme 5.5) is the same as the process of forming cyclopentenones, with the exception that the former terminal allylic carbon is attacked by the acylic carbon atom, and at the same time the Ni-acyl bond breaks and the Ni-internal allylic carbon bond forms. Also in this case the *concerted* path is found to be less energetically demanding than the *direct* path. The transition state structures for both routes were located and characterized and are shown in Figure 5.8. The computed energy difference between **6** and the transition state for the concerted path, **TS3**, is 16.4 kcal.mol^{-1} (18.1 kcal.mol^{-1} at the B3LYP//BLYP level), whereas the TS structure, **TS3a**, for

the direct path is 23.5 kcal.mol^{-1} (21.1 kcal.mol^{-1} at the B3LYP//BLYP level) above **6**. The product of this step is the square planar complex **8**, which is more stable than the reactants but less stable than the cyclopentenone analog. At the BLYP level complex **8** is 3.6 kcal.mol^{-1} above complex **7**, while at the B3LYP//BLYP level this difference increases to 10.6 kcal.mol^{-1}.

Both conclusions, higher energy for cyclohexenone formation and easy chelation with the ketone oxygen, are supported by experimental facts: cyclopentenones are generally found as products and only substitution at the internal olefinic carbon atom of the allylic system leads to partial or complete formation of cyclohexenones. On the other side, either transition states **TS2** and **TS2a** or intermediates **7** and **7a** preclude β-elimination, since the metal cannot be coplanar with the α-ketone hydrogen. As a consequence, unlike in other related processes,[41] β-eliminated products are not formed unless strong conformational effects are present.[42] In the cyclohexenone counterparts **TS3**, **TS3a** and **8**, the chelated ring should be disfavored and, consequently, β-elimination proceeds instead of a further carbonylation leading to aromatic final products.

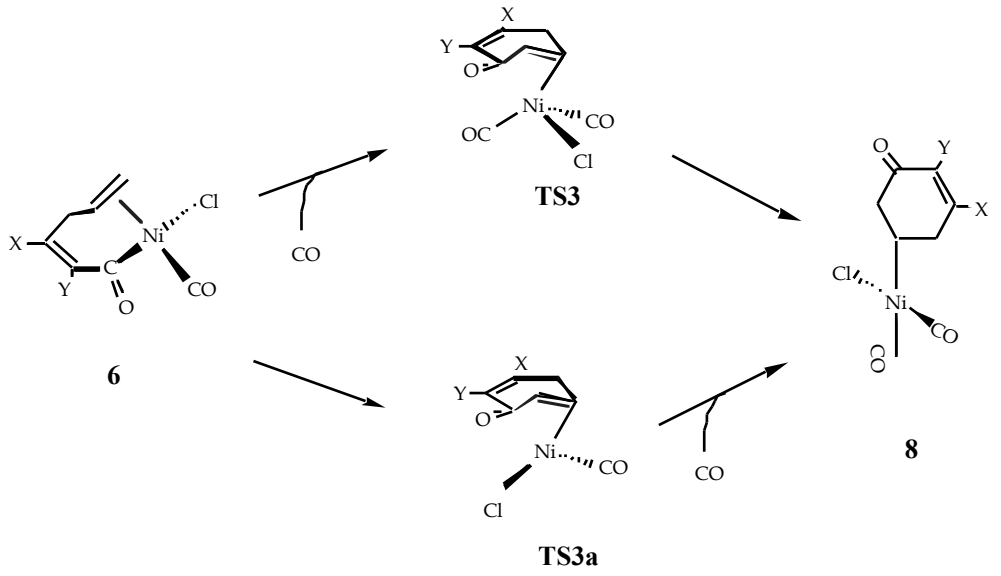

Scheme 5.5

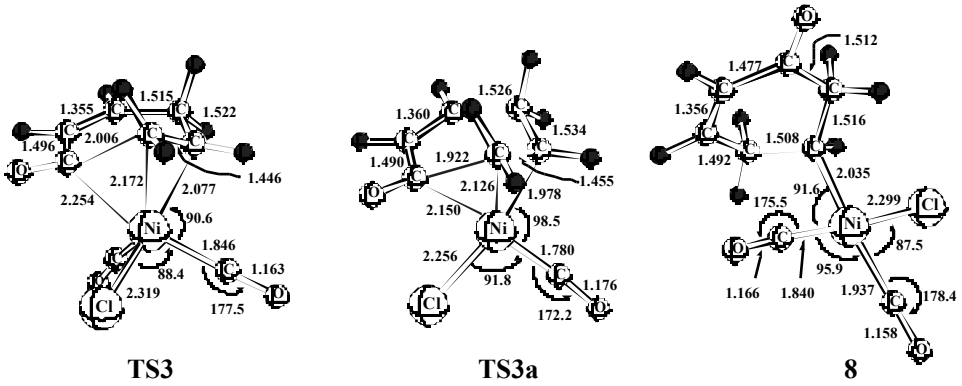

TS3 **TS3a** **8**

Figure 5.8. Selected geometric parameters for **TS3**, **TS3a**, and **8**.

5.3.5 Mechanism Energy Profile

Figure 5.9 shows the computed energy profile for the proposed mechanism. Computed energies at BLYP and at B3LYP//BLYP levels are presented. No qualitative differences between both levels of calculation were observed. At both levels of theory all relative energies are practically the same. The largest difference between both levels is found in the relative energies of complexes **7** and **8**. Zero point energies (ZPE) were evaluated for some structures and are also collected in Figure 5.9. None of the energy differences calculated including ZPE were modified by more than 1 or 2 kcal.mol^{-1}.

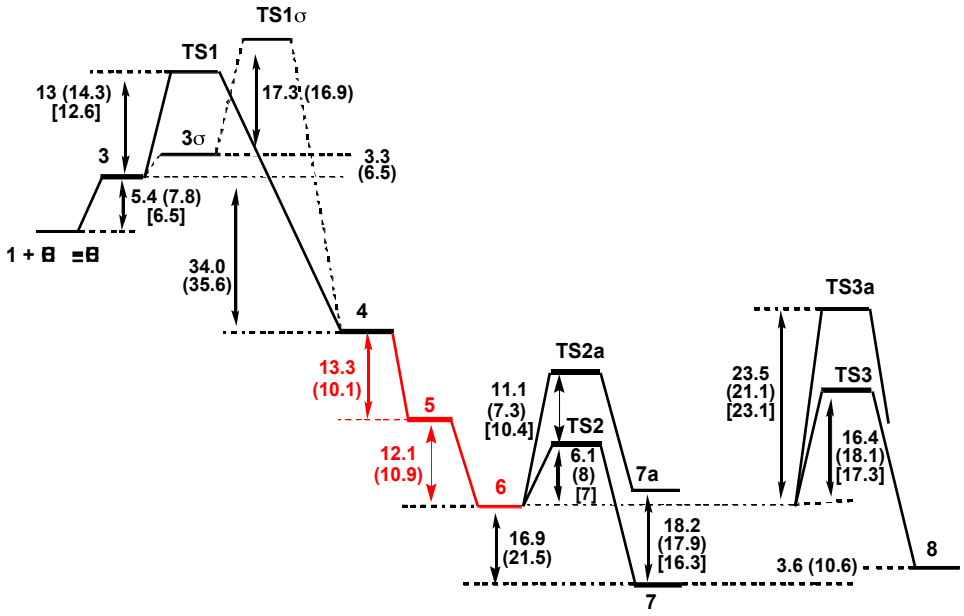

Figure 5.9. Reaction energy profile for the proposed mechanism. Energies without enclosures are at BLYP level, those in brackets are ZPE corrected at BLYP level, and those in parenthesis are at the B3LYP//BLYP level. All values are in kcal.mol^{-1}.

As we have discussed in the first section, the formation of the π-allyl complex **1** is endothermic. The amount of energy necessary to reach complex **1** from $Ni(CO)_4$ is 47.3 kcal.mol^{-1} at the BLYP level (38.2 kcal.mol^{-1} at the B3LYP//BLYP level). Note, however, that the overall reaction is highly exothermic and that the energy barriers are relatively low. In fact, once the TS structure **TS1** is reached, the process proceeds down hill to the products **7** or **8**. Thus, complex **7** is 71.2 kcal.mol^{-1} at the BLYP level (70.4 kcal.mol^{-1} at the B3LYP//BLYP) more stable than complex **1**.

The energy required to reach **TS1** from **1** and acetylene is 18.4 kcal.mol^{-1} at the BLYP level (22.1 kcal.mol^{-1} B3LYP//BLYP). This value is greater than the other two computed energy barriers, which close the cycle. The energy barrier to cyclopentenone formation is computed to be only 6.1 kcal.mol^{-1} at the BLYP level (8.0 kcal.mol^{-1} B3LYP//BLYP), whereas for cyclohexenones it is 16.4 kcal.mol^{-11} at the BLYP level (18.1 kcal.mol^{-1} B3LYP//BLYP). This result shows that cyclohexenones are more difficult to form than cyclopentenones or, in other words, that the reaction yield to six-member rings is lower than to five-member rings. As pointed out, these results fully agree with the experiment.

An interesting feature of this reaction mechanism is the alternation between four and five coordinated complexes. The intermediates that participate in the reaction mechanism are either 16- or 18-electron Ni(II) complexes. The coordinatively unsaturated 16e complexes, square planar or slightly distorted tetrahedral, can accept a new ligand: the alkyne or a carbonyl. The coordinatively saturated 18e complexes, square based pyramids, immediately react to produce a 16e complex that coordinates a new ligand and so on. This pattern is observed for the different steps: alkyne coordination and C–allyl–C–alkyne coupling, CO coordination and CO insertion, and CO coordination and ring-closing processes, although this last step is best viewed as a concerted reaction.

5.4 INFLUENCE OF ACETYLENE SUBSTITUTION

Moretó et al.[13b] showed that acetylene substituents have a dramatic influence on the product distribution. As we have mentioned above, the regioselectivity is determined in step **3** to **TS1**, that is, when the C-C bond between the acetylene and allyl is formed. When monosubstituted acetylenes are used, the products are mainly linear, whereas disubstituted acetylenes produce mainly cyclopentenones. In the latter case, it was found that the regioselectivity depends on alkyne triple bond polarization if the steric effects are not very demanding. It is assumed that this step is a nucleophilic attack of one acetylenic carbon on the allyl. Hence, it is expected that the more negatively charged the acetylenic carbon is, the more reactive it will be. In fact, experimental data supports this hypothesis. Table 5.1 shows the relative energies calculated for the two possible transition states for the coupling between the allyl and the acetylene, NPA and Mulliken atomic charges on acetylenic carbons, and experimental ^{13}C chemical shifts and relative conversions to the two possible isomers for some substituted acetylenes. The energy values reported in this section were computed at the BLYP level. Let us comment first on the experimental data taken from reference 13b. ^{13}C chemical shift values are roughly indicative of the electronic density around that atom. The atom least shifted is the most shielded one and, consequently, the one which is richest in electrons. Relative ^{13}C chemical shift values of acetylenic carbons have been used as a measure of the C-C triple bond polarization.[13b,44] The data in Table 5.1 show that the amount of product obtained by the attack of the least shifted atom on the allyl depends on the difference in the ^{13}C chemical shifts ($\Delta\delta$) of the two acetylenic carbons (the greater the difference, the more product is obtained). The cyclopentenonic products were distributed 90:0 when $\Delta\delta$ was 12.8 ppm and regioselectivity was poor when $\Delta\delta$ was 2.4 ppm. Thus, there is a nice correlation

between the acetylene triple bond polarization and the regioselectivity from this experimental data.

Table 5.1. Relative Energy for Different Transition States, Atomic Charges, ^{13}C Chemical Shifts and Distribution of Cyclopentenonic Products for Substituted Alkynes.

	ΔE^c		Q^d		$\delta(^{13}C)$				
$RC_1 \equiv C_2R'$	C_1-C_{allyl}	C_2-C_{allyl}	C1	C2	C1	C2	ΔQ^e	$\Delta\delta^f$	yield[a,g]
$HC \equiv CH$	0	0	-.225	-.225	71.9[b]	71.9[b]	.000	.000	
			(-.262)	(-.262)			(.000)		
$HC \equiv CCH_3$	0	3.4	-.240	-.027	66.9[b]	79.2[b]	.213	12.3	
			(-.459)	(.117)			(-.576)		
$FC \equiv CCH_3$	1.7	0	.376	-.188			-.564		
			(.041)	(-.064)			(-.105)		
$CH_3CO_2C \equiv CCH_3$			-.183	.072	72.8[a]	85.6[a]	.255	12.8	90/0
			(-.123)	(.015)			(.138)		
$CH_3COC \equiv CCH_3$			-.139	.076	81.7[a]	93.6[a]	.215	11.9	
			(-.084)	(-.021)			(.063)		
$CH_2OHC \equiv CCH_3$			-.067	.000	78.5[a]	81.6[a]	.067	3.1	46/10
			(-.036)	(-.062)			(-.026)		
$HC \equiv CCOCH_3$			-.134	-.134	79.4[a]	82.2[a]	.000	2.8	
			(-.401)	(.104)			(.505)		
$CH_3SCH_2C \equiv CCH_3$			-.057	.000	80.1[a]	82.5[a]	.057	2.4	30/18
			(-.044)	(-.065)			(-.021)		

[a] Values taken from ref 13b. [b] Values taken from ref 43. [c] Relative energy between the two **TS1**. [d] Calculated NPA atomic charges and Mulliken values in parenthesis. [e] Difference between atomic charges of C2 and C1. [f] Difference between ^{13}C chemical shifts of C2 and C1. [g] Yields in percent of the two possible cyclopentenonic products: C1-Callyl coupling/C2-Callyl coupling.

In order to test this hypothesis, several calculations were performed on free substituted acetylenes and the atomic charges were determined by means of two population analysis schemes, namely NPA (Natural Population Analysis) and Mulliken. The calculated atomic charges are shown in Table 5.1. The NPA charge differences between the acetylenic carbon atoms (ΔQ in Table 5.1) are in excellent agreement with the measured chemical shift trends ($\Delta\delta$ in Table 5.1). Such a strong correlation has been previously observed by other authors for phosphinoalkyne compounds.[45] The Mulliken values do not correlate as well as the NPA charges. At

this point, we can conclude that there is a strong correlation between NPA ΔQ values, ^{13}C $\Delta\delta$s and the observed regioselectivity.

As we have suggested above, this effect might be related to the reaction rate of the nucleophilic attack step. If such a relation exists, it could be manifested in the relative stability of the two transition states **TS1** that determine the regioselectivity. The mechanism proposed above involves the alkyne rotating to reach **TS1**. Depending on the direction of this rotation, one or the other product will be obtained. Thus, we determined **TS1** structures for propyne, and 1-fluoropropyne, as models for substituted alkynes with reversed triple bond polarization. The relative stability of the two **TS1** isomers for each substituted alkyne are collected in Table 5.1. For acetylene, both carbon atoms are obviously identical and have the same negative charge. When we replace a hydrogen atom with a methyl, the two carbon atoms are different and the nonsubstituted carbon more negatively charged than the substituted one. NPA and Mulliken charge values correlate well with ^{13}C shifts and the most charged atom is the less shifted. Likewise, the least charged atom is the most shifted. The relative energies required to reach each transition state were computed to be 0 and 3.4 kcal.mol^{-1} and these values agree very well with our hypothesis. In fact, the most negatively charged carbon atom attacks the allyl with the lowest barrier. Now, if we replace the methylacetylene H atom by a fluorine (third entry in Table 5.1), the acetylene triple bond changes its polarization. The atomic charges were determined by means of two methods (NPA and Mulliken) and indicate that now C2 is the most negatively charged; in this case, the energy barrier is lower for C2 than for C1. The relative stability of both transition state structures has now been reversed (C1 is 1.7 kcal.mol^{-1} above C2). Thus, the computed values for these model systems agree quite well with experimental trends, and justify the idea that regioselectivity is mainly determined by triple bond polarization.

5.5 INFLUENCE OF ALLYL SUBSTITUTION

Moretó et al.[13b] showed that allyl substitution had a considerable influence on product distribution. When the alkyne CH_3OCH_2-C_C-CH_3 was used with allyl bromide, no six-member ring product was observed, whereas cyclohexenone formation was detected in non-negligible amounts when 2-methylallyl bromide was used. In order to test if this effect could be attributed to a kinetic effect, we evaluated the differences between the energy barriers for the ring-closing steps and determined the TS structures **TS2** and **TS3** for a methyl-substituted allyl in position β. Let us remember that for the unsubstituted allyl we computed a

difference in the energy barriers of 10.4 kcal.mol^{-1} (at the BLYP level), the five-membered-ring closing process being less energy demanding than the six-membered-ring process (see Figure 5.9). For 2-methyl allyl, the relative ordering of both processes is unchanged, but the relative stability of the two TS's is reduced to 6.3 kcal.mol^{-1} (at the BLYP level). Thus, allyl substitution in position β reduces the difference between the energy barriers to cyclopentenones and to cyclohexenones.

5.6 CONCLUDING REMARKS

Using DFT calculations, a plausible mechanism for the carbonylative cycloaddition of allyl halides and acetylenes promoted by $Ni(CO)_4$ have been proposed. The first step is an oxidative addition of the allyl halide to a Ni(0) complex to form a Ni(II) π-allyl intermediate. Next, the alkyne coordinates to the metal and it readily attacks the allyl making the first new C-C bond. This step might also be carried out through σ-allyl intermediates. Then, a new CO coordinates to the metal and is inserted into the Ni-C bond to form an acylic species, which undergoes the ring closing process to form either cyclopentenones or cyclohexenones. The route to five-member ring products is found to be less energy demanding that the route to form cyclohexenones, in full agreement with experiment. An atomic charge based analysis demonstrates that regioselectivity is mainly determined by alkyne triple bond polarization. Indeed, the relative stability of the transition states that determine the regioselectivity depends on the alkyne polarization. Thus, the regioselectivity is manifested as a kinetic effect. Allyl substituents at β position decrease the difference between the barriers to cyclopentenones and cyclohexenones.

REFERENCES

1. Geis, O; Schmalz, H.G. *Angew. Chem. Int. Ed. Engl.* **1998**, *37*, 911-914
2. (a) Chiusoli, G.P.; Cassar, L., *Angew. Chem. Int. Ed. Engl.* **1967**, *6*, 124. (b) Chiusoli, G.P. *Acc. Chem. Res.* **1973**, *6*, 422-427
3. Khand, I.U.; Knox, G.R.; Pauson, P.L.; Watts, W.E., *J. Chem. Soc. Chem. Commun.* **1971**, 36.
4. (a) Hicks, F.A.; Buchwald, S.L. *J. Am. Chem. Soc.* **1996**, *118*, 11688-11689. (b) Hicks, F.A.; Kablaoui, N.M.; Buchwald, S.L. *J. Am. Chem. Soc.* **1996**, *118*, 9450-9451.
5. Agnel, G.; Negishi, E.-I.; *J. Am. Chem. Soc.* **1991**, *113*, 7424-7426.
6. (a) Jeong, N.; Lee, S.J.; Lee, J.L.; Chung, Y.K. *Tetrahedron Lett.* **1993**, *34*, 4027-4030. (b) Kent, J.L.; Wan, H.H.; Brummond, K.M. *Tetrahedron Lett.* **1995**, *36*, 2407-2410.
7. Hoye, T.R.; Suriano, J.A. *J.Am. Chem.Soc.* **1993**, *115*, 1154-1156
8. Pearson, A.J.; Dubbert, R.A.; *Organometallics* **1994**, *13*, 1656-1661
9. (a) Kondo, T.; Suzuki, N.; Okada, T.; Mitsudo, T. *J. Am. Chem. Soc.* **1997**, *119*, 6187-6118. (b) Chatani, N.; Morimoto, T.; Kukumoto, Y.; Murai, S. *J. Am. Chem. Soc.* **1998**, *120*, 5335-5336.
10. (a) Pagés, L.; Llebaria, A.; Camps, F.; Molins, E.; Miravitlles, C.; Moretó, J.M. *J. Am. Chem. Soc.* **1992**, *114*, 10449-10461. (b) Tamao, K.; Kobayashi, K.; Ito, Y. *Synlett.* **1992**, 539-546. (c) Zhang, M.H.; Buchwald, S.L. *J. Org. Chem.* **1996**, *61*, 4498-4499.
11. (a) Jeong, N.; Lee, S.; Sung, B.K., *Organometallics* **1998**, *17*, 3642-3644. (b) Koga, Y.; Kobayashi, T.; Narasaka, K. *Chem. Lett.* **1998**, 249-250.
12. For very recent references, see for instance: (a) Geis, O.; Schmalz, H.G. *Angew. Chem. Int. Ed. Engl.* **1998**, *37*, 911-914. (b) Witulsky, B.; Stengel T. *Angew. Chem. Int. Ed. Engl.* **1998**, *37*, 489-492 (c) Brummond, K.M.; Wan, H.; Kent, J.L. *J. Org. Chem.* **1998**, *63*, 6535-6545. (d) Belanger, D.B.; O'Mahony, D.J.R.; Livinghouse, T. *Tetrahedron Lett.* **1998**, *39*, 7637-7640. (e) Cadierno, V.; Gamasa, M.P.; Gimeno, J.; Moretó, J.M.; Ricart, S.; Roig, A.; Molins, E. *Organometallics* **1998**, *17*, 697-706. (f) Schick, U.; Jordi, L.; Ricart, S.; Veciana, J.; Dotz, K.H.; Moretó, J.M. *J. Am. Chem. Soc.* **1998**, *120*, 2283-2289. (g) Verdaguer, X.; Vázquez, J.; Fuster, G.; Bernardes-Génisson, V.; Greene, A.E.; Moyano, A.; Pericàs, M.A., Riera, A. *J. Org. Chem.* **1998**, *63*, 7037-7052. (h) Sugihara, T.; Yamaguchi, M. *J. Am. Chem. Soc.* **1998**, *120*, 10782-10783. (i) Mukai, C.; Kim, J.S.; Uchiyama, M.; Hanoaka, M.

Tetrahedron Lett. **1998**, *39*, 7909-7912. (j) Alcaide, B.; Polanco, C.; Sierra, M.A. *J. Org. Chem.* **1998**, *63*, 6786-6796. (k) Belanger, D.B.; Livinghouse, T. *Tetrahedron Lett.* **1998**, *39*, 7641-7644. (l) Ingate, S.T.; Marco-Contelles, *J. Org. Prep. Proc. Int.* **1998**, *30*, 121. (m) Kowalczyk, B.A.; Smith, T.C.; Dauben, W.G. *J. Org. Chem.* **1998**, *63*, 1379-1389. (n) Brummond, K.M.; Wan, H. *Tetrahedron Lett.* **1998**, *39*, 931-934. (o) Sugihara, T.; Yamada, M.; Ban, H.; Yamaguchi, M; Kaneko, C. *Angew. Chem. Int. Ed. Engl.* **1998**, *37*, 2801-2804. (p) Rajesh, T.; Periasamy, M. *Tetrahedron Lett.* **1998**, *39*, 117-118. (q) Gordon, C.M.; Kiszka, M.; Dunkin, I.R.; Kerr, W.J.; Scott, J.S.; Gebicki, J. *J. Organomet. Chem.* **1998**, *554*, 147-154.

13. (a) Camps, F.; Coll, J; Moretó, J.M.; Torras, J.M. *Tetrahedron Lett.* **1985**, *26*, 6397. (b) Camps, F.; Coll, J.; Moretó, J.M.; Torras, J. *J. Org. Chem.* **1989**, *54*, 1969-1978. (c) Camps, F.; Moretó, J.M.; Pagés, L.M. *Tetrahedron* **1992**, *48*, 3147-3162. (d) Llebaria, A.; Moretó, J.M. *J.Organomet. Chem.* **1993**, *451*, 1-13. (e) Oppolzer, W. *Pure Appl. Chem.* **1990**, *62*, 1941-1948 and references therein.
14. (a) Garcia-Gómez, G.; Moretó, J.M. *J. Am. Chem. Soc.* **1999**, *121*, 878-879. (b) Garcia-Gómez, G.; Moretó, J.M. *Inorg. Chim. Acta* **1999**, *296*, 94-102.
15. Ziegler, T., *Can. J. Chem.* **1995**, *73*, 743-761
16. For very recent references, see for instance: (a) Yoshizawa, K.; Shiota, Y.; Yamabe, T. *J. Am. Chem. Soc.* **1999**, *21*, 147-153. (b) Aranyos, A.; Szabo, K.J.; Backwall, J.E. *J. Org. Chem. 1998*, *63*, 2523-2529. (c) Hill, G.S.; Puddephatt, R.J. *Organometallics* **1998**, *17*, 1478-1486 (d) Torrent, M.; Deng, L.Q.; Ziegler, T. *Inorg. Chem.* **1998**, *37*, 1307-1314 (e) Torrent, M.; Deng, L.Q.; Duran, M.; Sola, M.; Ziegler, T. *Organometallics* **1997**, *16*, 13-19 (f) Reference 12g (g) Tobisch, S.; Bogel, H.; Taube, R. *Organometallics* **1998**, *17*, 1177-1196 (h) Pavlov, S.; Siegbahn, P.E.M.; Blomberg, M.R.A.; Crabtree, R.H. *J. Am. Chem. Soc.* **1998**, *120*, 548-555
17. (a) UNICHEM. Version 2.1-DGauss; Publication APG 5505-2.1; Cray Research Inc. Mendota Heights, 1993. (b) Gaussian 94. Revision B.3. Frisch, M.J.; Trucks, G.W.; Schlegel, H.B.; Gill, P.M.W.; Johnson B.G.; Robb, M.A.; Cheeseman, J.R.; Keith, T.; Petersson, G.A.; Montgomery, J.A.; Raghavachari, K.; Al-Laham, M.A.; Zakrzewski, V.G.; Ortiz, J.V.; Foresman, J.B.; Peng, C.Y.; Ayala, P.Y.; Chen, W.; Wong, N.W.; Andres, J.L.; Replogle, E.S.; Gomperts, R.; Martin, R.L.; Fox, D.J.; Binkley, J.S.; Defrees, D.J.; Baker, J.; Stewart, J.P.; Head-Gordon, M.; González, C. and Pople, J.A., Gaussian, Inc. Pittsburgh PA 1995
18. Godbout, N.; Salahub, D.R.; Andzelm, J.; Wimmer, E. *Can. J. Chem.* **1992**, *70*, 560.

19. Vosko, S.H.; Wilk, L.; Nusair, M. *Can. J. Phys.* **1980**, *58*, 1200.
20. (a) Becke, A.D. *Phys. Rev.A* **1988**, *38*, 3098. (b) Becke, A.D. *J. Chem. Phys.* **1988**, *88*, 2547.
21. Lee, C.; Yang, W.; Parr, R.G. *Phys. Rev. B* **1988**, *37*, 785.
22. González-Blanco, O; Branchadell, V. *J. Chem. Phys.* **1999**, *110*, 778.
23. Becke, A.D. *J. Chem. Phys.* **1993**, *98*, 5648.
24. Bader, R.F.W. *Atoms in Molecules. A Quantum Theory*; Clarendon Press: Oxford, 1990; Bader, R.F.W. Chem. Rev. **1992**, *91*, 893
25. Xaim has been developed by Jose Carlos Ortiz and Carles Bo. Universitat Rovira i Virgili. Tarragona. Spain. Xaim is freely available from the following address: http://www.quimica.urv.es/XAIM
26. Biegler-Konig, F.W.; Bader, R.F.W.; Tang, T.H. *J. Comput. Chem.* **1982**, *3*, 317.
27. Reed, A.E.; Weinstock, R.B.; Weinhold, F. *J.Chem.Phys.* **1985**, *83*, 735. Reed, A.E.; Weinhold, F. *J. Am. Chem. Soc.* **1986**, *108*, 3586.
28. Mulliken, R.S. *J.Chem.Phys.* **1955**, *23*, 1833
29. (a) Braga, D.; Grepioni, F.; Orpen, A.G., *Organometallics* **1993**, *12*, 1481. (b) Hedberg, L.; Ijima, T.; Hedberg, K., *J.Chem.Phys.* **1979**, *70*, 3224.
30. Li, J. ; Schreckenbach, G.; Ziegler, T. *J. Am. Chem. Soc.* **1995**, *117*, 486-494.
31. Stevens, A.E.; Feigerle, C.S.; Lineberger, W.C. *J. Am. Chem. Soc.* **1982**, *104*, 5026.
32. Goddard, R.; Kruger, C.; Mark, F.; Stansfield, R.; Zhang, X. *Organometallics* **1985**, *4*, 285.
33. Corey, E.J.; Semmelhack, M.F.; Hegedus, L.S.; *J. Am. Chem. Soc.* **1968**, *90*, 2416.
34. Brandes, H.; Goddard, R.; Jolly, P.W.; Kruger, C.; Mynott, R.; Wilke, *G. Z. Naturforsch, Teil B*, **1984**, *39*, 1139.
35. Carmona, E.; Marin, J.M.; Panaque, M.; Poveda, M.L.; *Organometallics,* **1987**, *6*, 1757.
36. 3D Search and Research using the Cambridge Structural Database, Allen, F.H.; Kennard, O. *Chemical Design and Automation News*, **1993**, *8*, 31-37.
37. Churchill, M.R.; O'Brien, T.A. *J. Am. Chem. Soc.* **1970**, 206.
38. The Ni-O bond strength has been evaluated as the energy difference between 10a and a new conformation of complex 10a without that interaction. This new conformation was generated by rotating 180° around the C-C bond.
39. Carmona, E.; Gutierrez-Puebla, E.; Monge, A.; Marin, J.M.; Paneque, M.; Poveda, M.L. *Organometallics* **1989**,*8*, 867.
40. (a) Zheng, P.-J. et al., *J. Struct.Chem.* **1992**, *11*, 321. (B) Giordano, T.J.; Palenik, G.J.; Palenik, R.C.; Sullivan, D.A. *Inorg.Chem.* **1979**, *18*, 244.

41. (a) Hayashi, T.; Tang, J.; Kato, K. *Org. Lett.* **1999**, *1*, 1487-1489. (b) Gabriele, B.; Salerno, G.; De Pascali, F.; Costa, M.; Chiusoli, G.P. *J. Org. Chem.* **1999**, *64*, 7693-7699.
42. Vilaseca, F.; Pagés, Ll.; Villar, J.M.; LLebaria, A.; Delgado, A.; Moretó, J.M. *J. Organomet. Chem.* **1998**, *551*, 107-115.
43. Tables for structural elucidation of organic compounds by spectroscopic methods. Pretsch, E.; Clerc, T.; Seibl, J.; Simon, W. Springer Verlag, 1976, Berlin-Heildelberg-New York.
44. Albright, T.A; Freeman, W.J.; Schweizer, E.E. *J. Am. Chem. Soc.* **1975**, *97*, 2946.
45. Louattani, E:; LLedos, A.; Suades, J.; Alvarez-Larena, A.; Piniella, J.F. *Organometallics* **1995**, *14*, 1053.